

Measurement of the ultrasound attenuation and dispersion in 3D-printed photopolymer materials from 1 to 3.5 MHz

Marina Bakaric,^{1,a),g)} Piero Miloro,^{2,b)} Ashkan Javaherian,^{1,c)} Ben T. Cox,^{1,d)} Bradley E. Treeby,^{1,e)} and Michael D. Brown^{1,f)}

¹Department of Medical Physics and Biomedical Engineering, University College London, Gower Street, London WC1E 6BT, United Kingdom

²Ultrasound and Underwater Acoustics, National Physical Laboratory, Hampton Road, Teddington TW11 0LW, United Kingdom

ABSTRACT:

Over the past decade, the range of applications in biomedical ultrasound exploiting 3D printing has rapidly expanded. For wavefront shaping specifically, 3D printing has enabled a diverse range of new, low-cost approaches for controlling acoustic fields. These methods rely on accurate knowledge of the bulk acoustic properties of the materials; however, to date, robust knowledge of these parameters is lacking for many materials that are commonly used. In this work, the acoustic properties of eight 3D-printed photopolymer materials were characterised over a frequency range from 1 to 3.5 MHz. The properties measured were the frequency-dependent phase velocity and attenuation, group velocity, signal velocity, and mass density. The materials were fabricated using two separate techniques [PolyJet and stereolithograph (SLA)], and included Agilus30, FLXA9960, FLXA9995, Formlabs Clear, RGDA8625, RGDA8630, VeroClear, and VeroWhite. The range of measured density values across all eight materials was 1120–1180 kg · m⁻³, while the sound speed values were between 2020 to 2630 m · s⁻¹, and attenuation values typically in the range 3–9 dB · MHz⁻¹ · cm⁻¹. © 2021 Acoustical Society of America. <https://doi.org/10.1121/10.0006668>

(Received 31 May 2021; revised 13 September 2021; accepted 21 September 2021; published online 14 October 2021)

[Editor: Christina Jeanne Naify]

Pages: 2798–2805

I. INTRODUCTION

The ability to arbitrarily control acoustic fields in 3D is vital to a diverse range of applications in biomedical ultrasound. Ultrasonic neuromodulation,¹ 3D ultrasound imaging,² therapeutic ultrasound,³ and particle or cell trapping⁴ all require a means of shaping a transmitted field in 3D. This is conventionally achieved using piezoelectric arrays. However, in recent years, the increasing ubiquity and quality of 3D printing has facilitated the development of a variety of different acoustic meta-materials and lenses as a cheaper alternative.^{5,6} One such approach is the generation of acoustic holograms.⁷ These are 3D-printed phase plates that are able to map the continuous wave output of a single-element transducer or array onto a pre-defined phase map via variations in sound speed and thickness. This phase map can be designed such that the wavefront diffracts to form an arbitrary distribution of acoustic pressure.^{8,9}

Compared to phased arrays, acoustic holograms are cheap to fabricate, require only a single element transducer, thus, simplifying the driving electronics, and offer higher fidelity control over the transmitted phase. One requirement, both for the design of acoustic holograms and other acoustic meta-materials, is the need for accurate knowledge of the acoustical properties of the 3D printing materials. This allows both for their behaviour to be accurately predicted and for their efficiency to be maximised for a particular application.¹⁰ However, while a number of works have reported these parameters,^{7,11–19} these measurements have typically been made at a single frequency, reported only sound speed, and or been carried out on a single or limited range of materials. A more recent work carried out detailed measurements on the properties of 3D-printed thermoplastics.²⁰ However, thermoplastics are not generally used for ultrasonic wavefront shaping due to their very high attenuation. Another work, by Jacquet *et al.*, measured both the attenuation and dispersion of several photopolymers more commonly used for acoustic hologram fabrication over the frequency range 15–55 MHz.²¹ Harmsen also measured the properties of a large range of photopolymers centred on 2.25 MHz; however, this work reported just the group velocity without measuring the attenuation and dispersion.²²

In the current work, the attenuation and dispersion of a set of eight 3D-printed photopolymer materials fabricated using a stereolithograph (SLA) and PolyJet printer were characterised over the frequency range 1–3.5 MHz. These measurements overlap with some of the materials investigated by

This paper is part of a special issue on ADDITIVE MANUFACTURING AND ACOUSTICS.

^{a)}Also at: Ultrasound and Underwater Acoustics, National Physical Laboratory, Hampton Road, Teddington TW11 0LW, UK. ORCID: 0000-0002-3609-311X.

^{b)}ORCID: 0000-0001-6809-2296.

^{c)}ORCID: 0000-0003-0798-3196.

^{d)}ORCID: 0000-0001-7296-4093.

^{e)}ORCID: 0000-0001-7782-011X.

^{f)}Also at: Department of Neuroscience, Erasmus MC, Dr. Molewaterplein 40, Rotterdam NL-3015 GD, Netherlands. ORCID: 0000-0002-0153-7403.

^{g)}Electronic mail: marina.bakaric.16@ucl.ac.uk

Jacquet *et al.* but cover a different frequency range for which different attenuation mechanisms might be dominant.²¹ These data will prove valuable to researchers aiming to optimise the design of acoustic holograms and other meta-materials. Beyond this specific application to wavefront shaping, the photopolymers characterised in this work have also been used for a range of other biomedical applications, including the generation of complex 3-D bone mimicking imaging phantoms,^{21,23} teaching phantoms,²⁴ and acoustic absorbers.¹⁹

II. METHODS

A. Materials

The materials chosen were eight photopolymers fabricated using two 3D printers covering a range of mechanical properties. The materials were printed at The Bartlett Manufacturing and Design Exchange [B-made, The Bartlett School of Architecture, University College London, London, UK (UCL)] using two printing techniques, namely PolyJet (Objet) multi-polymer printing, and stereolithography (SLA). A Stratasys J835 (Stratasys, Edina, MN, US) was used to print the Agilus30, FLXA9960, FLXA9995, RGDA8625, RGDA8630, VeroClear, and VeroWhite samples. Of these Agilus30, VeroClear, and VeroWhite are “primary” materials designed to simulate either poly(methyl methacrylate) (PMMA) (VeroClear, VeroWhite) or a rubber-like material (Agilus30), respectively. The materials FLXA9960, FLXA9995, RGDA8625, and RGDA8630 are “digital” materials formed by mixing pre-determined ratios of VeroClear and Agilus30 to generate a range of mechanical properties. A Formlabs Form 3 (Formlabs, Somerville, MA, US) was used for the Formlabs Clear resin samples.

Two samples of each material were printed as discs with a diameter of 60 mm and nominal thicknesses of 4 and 8 mm, as required for the through-transmission, two-sample substitution measurements,²⁵ described in Sec. II C.

B. Density Measurement

The density of the 3D-printed samples was determined from measurements of mass and sample volumes. The mass of each sample was measured using a ML203T/00 precision balance (Mettler Toledo, Columbus, OH, USA) with a resolution of 1 mg. The sample dimensions (diameter and thickness) were measured using a digital precision caliper (Mitutoyo, Tokyo, Japan) with a resolution of 0.01 mm, and the volume calculated as $V = \pi r^2 L$, where r is the sample radius and L is the sample thickness, expressed in meters. The sample mass, diameter, and thickness were measured five times and the mean \pm standard deviation used to calculate the density.

C. Insertion Loss and Sound Speed Measurement

Acoustic properties of the materials were characterized using a broadband through-transmission setup^{25,26} available at the NPL Materials Measurement Facility (National Physical Laboratory, Teddington, UK) and shown in Fig. 1.

Sound speed and insertion loss were measured using a two-sample substitution technique with reference to de-ionised water.²⁷ The temperature during the measurements was $19.5 \text{ }^\circ\text{C} \pm 0.5 \text{ }^\circ\text{C}$, measured using a calibrated spirit-in-glass thermometer (IP39C, G. H. Zeal, London, UK). A single-element broadband transducer with a centre frequency of 2.25 MHz and active diameter of 13 mm (Olympus, Waltham, MA, USA) was used as the emitter, while a 30 mm active element diameter broadband bilaminar hydrophone (GEC-Marconi, Essex, UK) was used as a receiver. The devices were connected to an Olympus 5073PR pulser-receiver (Olympus, Waltham, MA, USA), with typical settings of gain +10 dB, pulse repetition frequency 1 kHz, energy 4, and damping 1. The recorded acoustic signals were digitised using a Tektronix DPO7254 Digital Phosphor Oscilloscope (Tektronix UK, Bracknell, UK) with a time window of 5 μs , sampling rate of 2.5 GSamples/s, 12 500 samples, and 5000 averages. Before each acquisition, the peak negative pressure of the pulse was aligned to the centre of the time window (see Fig. 2). The signals were stored using an in-house developed LabVIEW (National Instruments, Austin, TX, USA) software and later processed in MATLAB (MathWorks, Natick, MA, USA) (see Sec. II D).

In order to derive the required acoustic properties, a pair of acoustic pulses was recorded for each sample: (i) the water path transmission signal (or reference), and (ii) the through-sample transmission signal acquired by positioning the sample in the acoustic path. Along with the sample thickness values, this set of measurements allows the

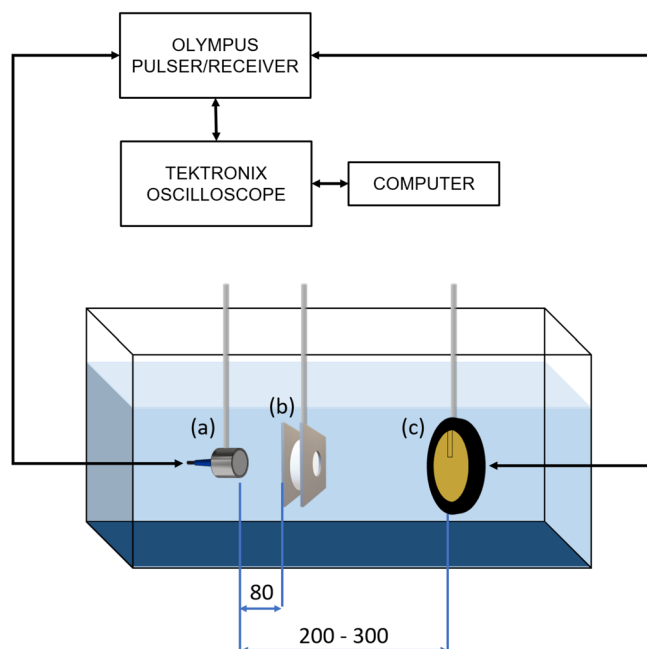


FIG. 1. (Color online) Measurement setup used to determine the speed of sound and attenuation. (a) Transmitter/receiver transducer, (b) PMMA sandwich holder with the sample, and (c) Membrane hydrophone used to detect the ultrasound transmitted through the sample. The typical distances are indicated in millimetres.

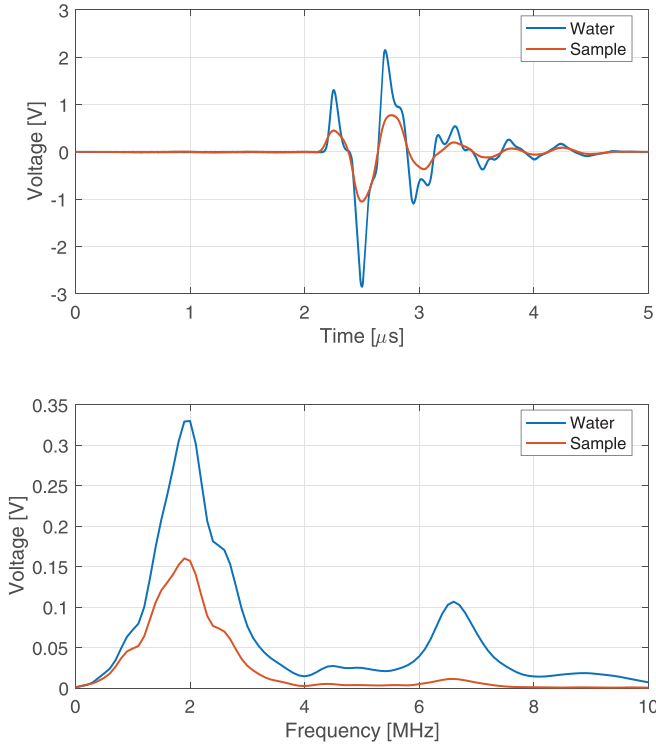


FIG. 2. (Color online) (a) Example of a pair of recorded signals (with and without the sample) for an 8 mm sample of VeroClear. (b) Corresponding single-sided amplitude spectra. The second peak arises at the third harmonic of the transducer resonance frequency (2.25 MHz) due to the very short pulsed excitation.

simultaneous evaluation of insertion loss and sound speed as described by Rajagopal *et al.*²⁷ In order to derive attenuation from the insertion loss measurements, two samples for each material with nominal thicknesses of 4 and 8 mm were used.²⁷ The samples were held in a sandwich holder made of PMMA, with acoustic windows of 50 mm diameter. The aperture size was such that no acoustic reflections of the acoustic beam were generated from the holder. The samples were aligned by maximizing the magnitude of the reflection from the sample front interface by using a five degrees-of-freedom translation stage.

Four independent sets of measurements were acquired for each sample by changing the pulser energy once, and the axial transmitter–receiver separations twice. This is done to exclude any possible contributions from diffraction and nonlinear effects.²⁷ Thus, for each material, a set of eight repetitions were performed (two different sample thicknesses and four measurements at different distances/pulser settings each). Typical transmitter–receiver separations used were in the range from 200 to 300 mm, while the distance between the transmitter and the front face of the sample was on the order of 80 mm.

D. Signal Processing

For each material, the recorded time-domain signals were processed in MATLAB by first removing any DC offset (by setting the DC component to zero in the Fourier spectrum) and then filtering the time-domain signals using a Tukey (tapered-cosine) window with a cosine fraction of 0.25.

The signals were then Fourier transformed using a zero-padded fast Fourier transform (FFT) and the single-sided amplitude $A(f)$ and phase $\phi(f)$ spectra were obtained as a function of frequency f . An example of a pair of recorded signals and their amplitude spectra is shown in Fig. 2.

The insertion loss IL (which includes all losses due to the insertion of the sample) in dB for each pair of water-sample signals was calculated by

$$IL(f) = -20 \log_{10} \left(\frac{A_s(f)}{A_w(f)} \right). \quad (1)$$

The attenuation (which includes contributions from both absorption and scattering), was then calculated from the average IL across the four repeated measurements for each of the thin and thick samples, where

$$\alpha(f) = \frac{IL_{\text{thick}}(f) - IL_{\text{thin}}(f)}{L_{\text{thick}} - L_{\text{thin}}} + \alpha_w(f). \quad (2)$$

Here, $\alpha(f)$ is the frequency-dependent attenuation in units of $\text{dB} \cdot \text{cm}^{-1}$, L is the sample thickness in cm, and α_w is the frequency-dependent attenuation in water calculated using a 7th-order polynomial fit to the data in Pinkerton²⁸ (this fit is available via the waterAbsorption function in the k-Wave Toolbox).²⁹

The frequency-dependent phase velocity (or dispersion) was calculated by first unwrapping the phase values and then adding the linear component of the phase due to the offset of the recorded time window (i.e., adding $2\pi ft_0$ to the unwrapped phase, where t_0 is the time at the beginning of the recorded time window for that signal). The phase velocity for each pair of water-sample measurements was then calculated using³⁰

$$c_p(f) = \frac{2\pi fL}{2\pi fL/c_w - (\phi_w(f) - \phi_s(f))}, \quad (3)$$

where L is the sample thickness, and c_w is the sound speed in water calculated using the 5th order polynomial fit given in Marczak³¹ (this fit is available via the waterSoundSpeed function in the k-Wave Toolbox²⁹) Finally, the average phase velocity for each material was calculated by taking the mean across all eight pairs of measurements (two samples of different thicknesses, four repeats for each sample).

A power law fit to the calculated frequency-dependent attenuation $\alpha(f)$ and dispersion $c_p(f)$ was obtained by simultaneously fitting the data to the analytical expressions^{32,33}

$$\alpha_{\text{fit}}(f) = \alpha_0 f^y \quad (4)$$

$$c_{p,\text{fit}}(f) = \left(\frac{1}{c_{\text{ref}}} + \alpha_{0,\text{np}} \tan(\pi y/2) \left(\omega^{y-1} - \omega_{\text{ref}}^{y-1} \right) \right)^{-1}, \quad (5)$$

where α_0 and $\alpha_{0,\text{np}}$ are the power law attenuation prefactor in units of $\text{dB} \cdot \text{MHz}^{-y} \cdot \text{cm}^{-1}$ and $\text{Np} \cdot (\text{rad} \cdot \text{s}^{-1})^{-y} \cdot \text{m}^{-1}$, respectively, $\omega = 2\pi f$, and c_{ref} is the sound speed at the

reference frequency $f_{\text{ref}} = 2$ MHz. The attenuation and dispersion in a causal medium are linked by the Kramers–Kronig relations,³⁴ and thus fitting to both parameters simultaneously improves the robustness of the fit.³⁵ The scalar parameters α_0 , y , and c_{ref} were fitted to the measured data over the frequency range 1.5–3 MHz using a simplex method (fminsearch in MATLAB) by minimising the objective function

$$E = \frac{\sum_f (\alpha(f) - \alpha_{\text{fit}}(f))^2}{\alpha(f)^2} + \frac{\sum_f (c_p(f) - c_{p,\text{fit}}(f))^2}{c_p(f)^2}. \quad (6)$$

The square of the mean values is used in the denominator to normalise the contributions from the attenuation and dispersion misfit to the objective function.

Given the power law fit for the frequency-dependent phase velocity c_p in Eq. (5), the group velocity c_g (the speed at which the overall envelope of the wave travels) can be calculated directly from the gradient of the phase velocity with respect to the frequency³⁶

$$c_g = c_a \left[1 - \frac{\omega_a}{c_a} \left(\frac{\partial c_p}{\partial \omega} \right)_{\omega_a} \right]^{-1}, \quad (7)$$

where the subscript a signifies the scalar values at the centre frequency of the pulse (in this case 2 MHz). Applying this expression to Eq. (5) then gives

$$c_g = \left[\frac{1}{c_a} + \frac{(y-1)}{c_a^2} c_{\text{ref}} \alpha_{0,\text{np}} \omega_a^{y-1} \tan(\pi y/2) \right]^{-1}. \quad (8)$$

If c_a is taken as c_{ref} (the fitted phase velocity at 2 MHz), then this simplifies to

$$c_g = \frac{c_{\text{ref}}}{1 + (y-1) \alpha_{0,\text{np}} \omega_a^{y-1} \tan(\pi y/2)}. \quad (9)$$

In most cases, $c_g \approx c_{\text{ref}}$ as the second factor in the denominator in Eq. (9) is small.

In addition to the group velocity, the signal velocity (the speed at which the very front edge of the propagating

wave travels) was also calculated. The first time of arrival was calculated based on the Akaike information criterion.³⁷ The scalar signal velocity was then calculated for each pair of measurements using

$$c_{\text{sig}} = \frac{L}{L/c_w - (t_w - t_s)}, \quad (10)$$

where t_w and t_s are the extracted time of flight for the measurement in water and with the sample present, respectively [note the similarity to Eq. (3)]. The reported values for the signal velocity were again averaged across all eight pairs of measurements for each material.

E. Uncertainties

The measurement uncertainty was evaluated following the UK Accreditation Service guide to the expression of uncertainty and confidence in measurement.³⁸ The type A standard uncertainties quoted in the Results section were determined according to the methods recommended in Refs. 8 and 39. The type A error of insertion loss and phase velocity were calculated as the standard deviation of the four measurement repetitions for each sample, divided by the square root of the number of repetitions. The type A error of density and attenuation was determined using the combined standard uncertainty for uncorrelated quantities.³⁹ Systematic effects arising from uncertainty in sample thickness are a dominant source of measurement error for all derived material properties, with an average uncertainty of approximately 0.25%. The exception is Agilus30 with a type A error of 0.5%, most probably due to its flexible, rubber-like structure, making it more challenging to measure its thickness. Other sources of uncertainty, including temperature and instrumentation, have been evaluated according to Ref. 26. Uncertainties are reported as expanded values with a coverage factor $k = 2$ and a coverage probability of 95%.

III. RESULTS

A. Measurement results

The measured properties for the eight 3D-printed photopolymers are summarised in Table I. The range of measured values across all eight materials was relatively small for

TABLE I. Measured acoustic properties of the 3D-printed photopolymers.^{a)}

	ρ_0 [kg · m ⁻³]	c_g [m · s ⁻¹]	c_{sig} [m · s ⁻¹]	c_{ref} [m · s ⁻¹]	α_0 [dB · MHz ^{-y} · cm ⁻¹]	y
Agilus30	1128	2035	2089	2035	9.109	1.017
FLXA9960	1125	2019	2108	2019	7.224	1.019
FLXA9995	1166	2166	2238	2166	5.766	0.9749
Formlabs	1178	2591	2629	2591	2.922	1.044
RGDA8625	1174	2457	2502	2457	3.894	0.8489
RGDA8630	1176	2447	2493	2447	3.933	0.9613
VeroClear	1181	2473	2512	2473	3.696	0.9958
VeroWhite	1175	2495	2560	2495	3.158	1.383

^{a)}Here, ρ_0 is the mass density, c_g is the group velocity, c_{sig} is the signal velocity, c_{ref} is the velocity obtained from the power law fit at the reference frequency $f_{\text{ref}} = 2$ MHz, α_0 is the power law attenuation prefactor, and y is the power law attenuation exponent. All values given to four significant figures.

density values which ranged between 1120 to 1180 kg · m⁻³ with a type A uncertainty of 5% for all samples except for Agilus30, for which the uncertainty was 10% due to the higher uncertainty in sample thickness, as described in Sec. IIE. The sound speed values were between 2020 to 2630 m · s⁻¹ with an expanded uncertainty of around 0.5%–0.6% (1% for Agilus30) across the entire frequency range, and the attenuation values typically in the range 3–9 dB · MHz⁻¹ · cm⁻¹. Expanded uncertainty was evaluated as in Ref. 26 to be 5% for all materials.

The frequency-dependent attenuation and phase velocity are shown in Figs. 3 and 4. The attenuation and dispersion for seven of the eight materials follow an approximately linear power law. The fitted power law curves generally agree well with both the attenuation and phase velocity data, especially in the frequency range closest to the transducer central frequency (1.5 to 2.5 MHz), where the signal-to-noise is the highest. At lower frequencies (below 1.5 MHz), the measured phase velocities deviate from the power law dispersion curves, but typically have

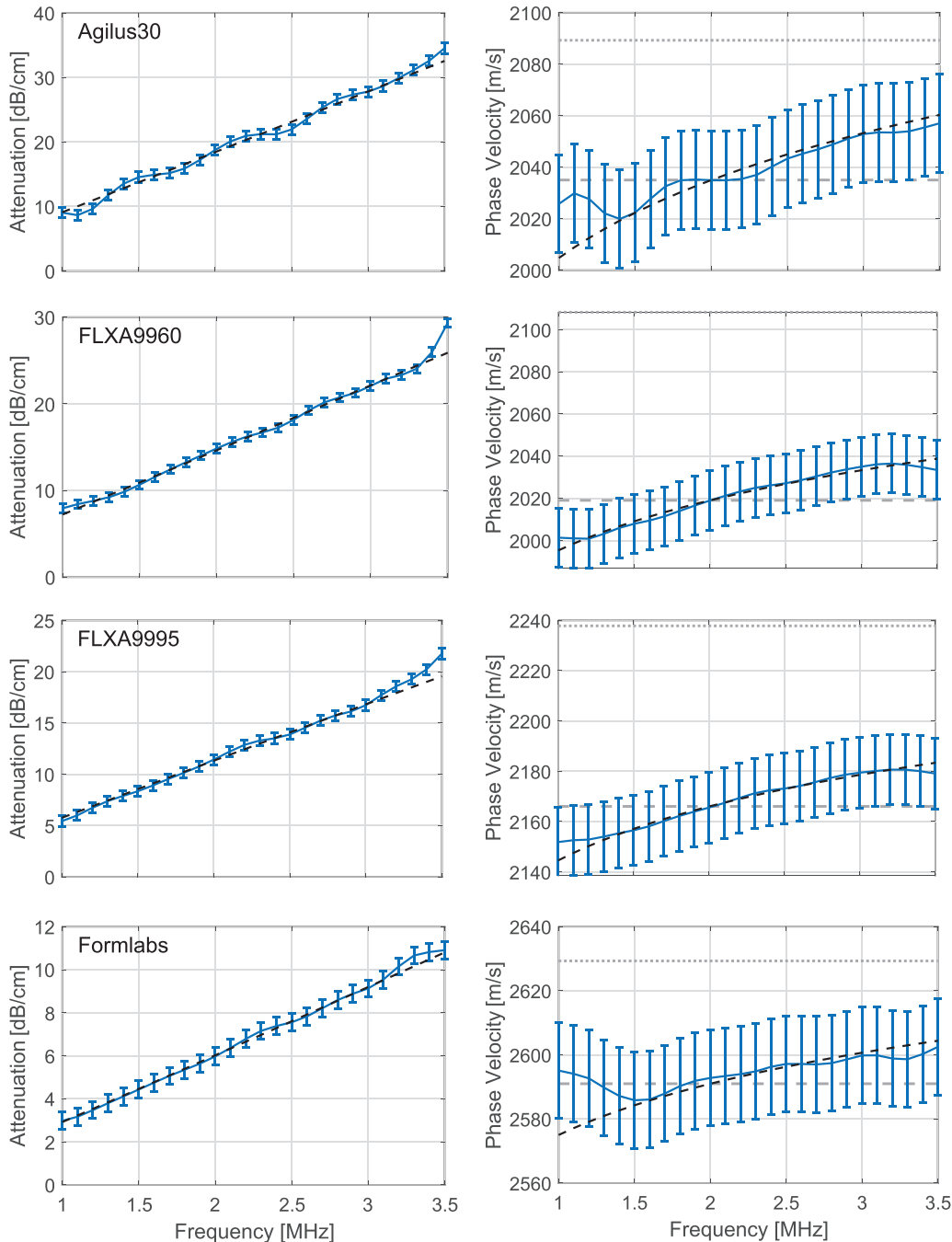


FIG. 3. (Color online) Attenuation (left panels) and phase velocity (right panels) for the first four of the tested 3D-printed photopolymers from Table I. The solid lines show the calculated values along with the type A uncertainty. The black dashed lines show the fitted power law model (fitted to the data from 1 to 3 MHz). The gray dashed and dotted lines on the phase velocity plots show the group velocity and signal velocity, respectively, for comparison.

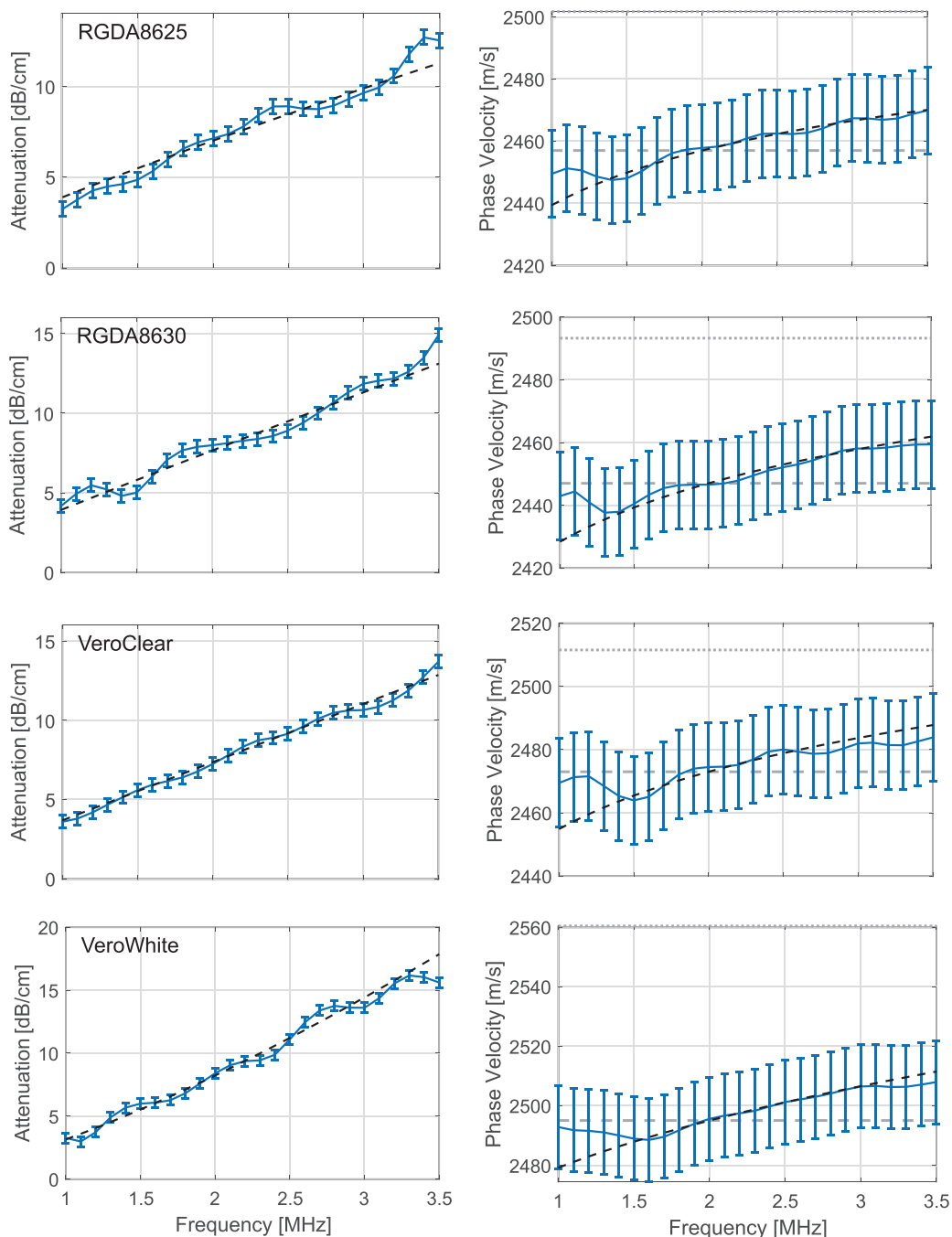


FIG. 4. (Color online) Attenuation (left panels) and phase velocity (right panels) for the second four of the tested 3D-printed photopolymers from Table I. The solid lines show the calculated values along with the type A uncertainty. The black dashed lines show the fitted power law model (fitted to the data from 1 to 3 MHz). The gray dashed and dotted lines on the phase velocity plots show the group velocity and signal velocity, respectively, for comparison.

higher uncertainty. Note, the precise values of the fitted power law parameters are sensitive to the frequency range chosen for the fit, as well as experimental uncertainties. Thus, while the fits match the experimental data fairly closely, not too much emphasis should be placed on small variations between the power law exponent for the different materials.

Overall, the results show that for the PolyJet samples, there is a clear distinction between the rubber-like materials (Agilus30, FLXA9960, FLXA9995) and the more rigid PMMA-like materials (VeroClear, VeroWhite, RGDA8625,

RGDA8630). The rubber-like materials have a higher acoustic attenuation and lower sound speed in the frequency range covered. For the rubber-like materials, there is also a clear decrease in attenuation and increase in signal velocity as the Shore-A hardness (values given in brackets) increases, e.g., from Agilus30 (30–40) → FLXA9960 (45–50) → FLXA9995 (92–95).⁴⁰ Between the PolyJet materials and the Formlabs resin, the Formlabs Clear has lower attenuation across the frequency range measured and greater sound speed, and so may represent the best choice for the fabrication of single material acoustic holograms.

Comparing the measured velocities, the signal velocity (the speed of the front edge of the propagating wave) is always higher than the group velocity (the speed of the envelope of the wave) as the measured traces also contain higher frequency information at the third harmonic (see Fig. 2), which has a higher phase velocity than the lower frequency components around the transducer centre frequency. The reference sound speed (which corresponds to the phase velocity of the fitted dispersion curve at 2 MHz) is typically very close to the calculated group velocity. If a single value of sound speed is needed for ultrasound frequencies in the 1–3.5 MHz range, the group velocity or reference velocity are likely to be the most suitable choice.

B. Comparison with Previously Published Results

There are several previous studies that report some of the properties measured in the current work. First, the material densities for several of the materials are available from the manufacturer website.^{40,41} These include Agilus30 (1140–1150 kg·m⁻³), Formlabs Clear (Somerville, MA, USA) (1150–1200 kg·m⁻³), VeroClear (1180–1190 kg·m⁻³) and VeroWhite (1170–1180 kg·m⁻³). The measured sample densities generally fall within the reference range reported by the manufacturer, and are between 1100 and 1200 kg·m⁻³, with the type A uncertainty ranging between 50 and 100 kg·m⁻³.

Robertson *et al.* reported measurements for VeroBlack (another photopolymer similar in composition to VeroWhite) of $c_g = 2495 \text{ m} \cdot \text{s}^{-1}$, $\alpha = 3.7 \text{ dB} \cdot \text{cm}^{-1}$ at 1 MHz (extrapolated based on measurements made at 5 MHz), and $\rho = 1180 \text{ kg} \cdot \text{m}^3$, which are very close to the values for VeroWhite reported in Table I.²³ For VeroClear, a higher sound speed and attenuation ($1.7 \text{ dB} \cdot \text{cm}^{-1}$) were found at 2 MHz compared to values reported by Melde *et al.*,⁷ though Melde *et al.* employed a different printer model for fabrication which could account for some of the discrepancy.

The group velocities for all seven PolyJet materials also fall within the values reported by Harmsen ($\pm 60 \text{ m} \cdot \text{s}^{-1}$)²² with the exception of FLXA9960. A lower attenuation power law exponent γ was found for VeroWhite compared to Jaquet *et al.* (1.38 versus 1.77).²¹ The two measurements, however, cover a different frequency range (1–3.5 MHz versus 15–55 MHz) and previous works have found differences in the power law frequency dependence over different bandwidths.³⁵ In particular, the contribution of scattering to the attenuation, e.g., due to impurities, density variations, or structures formed during the 3D printing process, may vary over different frequency ranges. For Formlabs Clear, close agreement is found with values reported at 0.5 MHz by Jimenez-Gambin *et al.*⁴² of $2580 \text{ m} \cdot \text{s}^{-1}$ and $1.38 \text{ dB} \cdot \text{cm}^{-1}$.

IV. SUMMARY

The acoustic properties of eight 3D-printed photopolymer materials widely used for wavefront shaping applications in biomedical ultrasound were measured over a frequency range from 1 to 3.5 MHz. The materials were

Agilus30, FLXA9960, FLXA9995, Formlabs Clear, RGDA8625, RGDA8630, VeroClear, and VeroWhite, and the properties measured were the frequency-dependent phase velocity and attenuation, group velocity, signal velocity, and mass density.

ACKNOWLEDGMENTS

This work was supported by the Engineering and Physical Sciences Research Council, UK.

- ¹G. Maimbourg, A. Houdouin, T. Deffieux, M. Tanter, and J. F. Aubry, “3D-printed adaptive acoustic lens as a disruptive technology for transcranial ultrasound therapy using single-element transducers,” *Phys. Med. Biol.* **63**(2), 025026 (2018).
- ²P. Kruizinga, P. van der Meulen, A. Fedjajevs, F. Mastik, G. Springeling, N. de Jong, J. G. Bosch, and G. Leus, “Compressive 3D ultrasound imaging using a single sensor,” *Sci. Adv.* **3**(12), e1701423 (2017).
- ³S. Bobkova, L. Gavrilov, V. Khokhlova, A. Shaw, and J. Hand, “Focusing of high-intensity ultrasound through the rib cage using a therapeutic random phased array,” *Ultrasound Med. Biol.* **36**(6), P888–906 (2010).
- ⁴M. Baudoin, J. L. Thomas, R. A. Sahely, J. C. Gerbodoen, Z. Gong, A. Sivery, O. B. Matar, N. Smagin, P. Favreau, and A. Vlandas, “Spatially selective manipulation of cells with single-beam acoustical tweezers,” *Nat. Commun.* **11**(1), 4244 (2020).
- ⁵C. Choi, S. Bansal, N. Münzenrieder, and S. Subramanian, “Fabricating and assembling acoustic metamaterials and phononic crystals,” *Adv. Eng. Mater.* **23**(2), 2000988 (2021).
- ⁶H. Ge, M. Yang, C. Ma, M. H. Lu, Y. F. Chen, N. Fang, and P. Sheng, “Breaking the barriers: Advances in acoustic functional materials,” *Nat. Sci. Rev.* **5**(2), 159–182 (2018).
- ⁷K. Melde, A. G. Mark, T. Qiu, and P. Fischer, “Holograms for acoustics,” *Nature* **537**(7621), 518–522 (2016).
- ⁸M. D. Brown, B. T. Cox, and B. E. Treeby, “Design of multi-frequency acoustic kinoforms,” *Appl. Phys. Lett.* **111**(24), 244101 (2017).
- ⁹M. D. Brown, “Phase and amplitude modulation with acoustic holograms,” *Appl. Phys. Lett.* **115**(5), 053701 (2019).
- ¹⁰M. Ferri, J. M. Bravo, J. Redondo, S. Jiménez-Gambín, N. Jiménez, F. Camarena, and J. V. Sánchez-Pérez, “On the evaluation of the suitability of the materials used to 3D print holographic acoustic lenses to correct transcranial focused ultrasound aberrations,” *Polymers* **11**(9), 1521 (2019).
- ¹¹R. Lirette and J. Mobley, “Focal zone characteristics of stepped Fresnel and axicon acoustic lenses,” *Proc. Meet. Acoust.* **31**(1), 045001 (2017).
- ¹²S. Jiménez-Gambín, N. Jiménez, J. M. Benlloch, and F. Camarena, “Holograms to focus arbitrary ultrasonic fields through the skull,” *Phys. Rev. Appl.* **12**(1), 014016 (2019).
- ¹³E. J. Alles, D. Nikitichev, and A. E. Desjardins, “Fabrication and Characterisation of Miniature Parabolic Acoustic Lenses,” in *International Ultrasonics Symposium (IUS), 2015 IEEE* (Taipei, 2015), pp. 3–6.
- ¹⁴A. Franklin, A. Marzo, R. Malkin, and B. W. Drinkwater, “Three-dimensional ultrasonic trapping of micro-particles in water with a simple and compact two-element transducer,” *Appl. Phys. Lett.* **111**(9), 094101 (2017).
- ¹⁵M. D. Fariñas, T. E. Álvarez-Arenas, G. Cummins, M. P. Desmulliez, V. Seetohul, and S. Cochran, “Assessment of the Ultrasonic Properties of Additive Manufactured Materials for Passive Components of Piezoelectric Transducers,” in *IEEE International Ultrasonics Symposium, IUS, Vol. 2016-November*, 2016.
- ¹⁶J. R. Jacquet, F. Levassort, F. Ossant, and J. M. Gregoire, “3D printed phantom for high frequency ultrasound imaging,” in *2015 IEEE International Ultrasonics Symposium, IUS 2015, Taipei, Taiwan* (2015), Vol. October 2019, pp. 1–4.
- ¹⁷C. Bai, M. Ji, A. Bouakaz, Y. Zong, and M. Wan, “Design and characterization of an acoustically and structurally matched 3-D-printed model for transcranial ultrasound imaging,” *IEEE Trans. Ultrason. Ferroelectr. Freq. Control* **65**(5), 741–748 (2018).

- ¹⁸R. Livings, V. Dayal, and D. Barnard, "Characterization of 3D rapid prototyped polymeric material by ultrasonic methods," *AIP Conf. Proc.* **1650**, 807–816 (2015).
- ¹⁹F. Acquaticci, M. M. Yommi, S. N. Gwirc, and S. E. Lew, "Rapid prototyping of pyramidal structured absorbers for ultrasound," *Open J. Acoust.* **07**(03), 83–93 (2017).
- ²⁰A. Antoniou, N. Evripidou, M. Giannakou, G. Constantinides, and C. Damianou, "Acoustical properties of 3D printed thermoplastics," *J. Acoust. Soc. Am.* **149**(4), 2854–2864 (2021).
- ²¹J.-R. Jacquet, F. Ossant, F. Levassort, and J.-M. Grégoire, "3-D-Printed phantom fabricated by photopolymer jetting technology for high-frequency ultrasound imaging," *IEEE Trans. Ultrason. Ferroelectr. Freq. Control* **65**(6), 1048–1055 (2018).
- ²²S. Harmsen, "Acoustic impedance matching using 3D printed lenses," B.S. thesis, University of Twente, Twente, Netherlands, 2018.
- ²³J. Robertson, E. Martin, B. Cox, and B. E. Treeby, "Sensitivity of simulated transcranial ultrasound fields to acoustic medium property maps," *Phys. Med. Biol.* **62**, 2559–2580 (2017).
- ²⁴S. Campelo, E. Subashi, S. G. Meltsner, Z. Chang, J. Chino, and O. Craciunescu, "Multimaterial three-dimensional printing in brachytherapy: Prototyping teaching tools for interstitial and intracavitary procedures in cervical cancers," *Brachytherapy* **19**(6), 767–776 (2020).
- ²⁵B. Zeqiri, W. Scholl, and S. P. Robinson, "Measurement and testing of the acoustic properties of materials: A review," *Metrologia* **47**(2), S156–S171 (2010).
- ²⁶R. M. Baêso, R. P. Costa-Felix, P. Miloro, and B. Zeqiri, "Ultrasonic parameter measurement as a means of assessing the quality of biodiesel production," *Fuel* **241**, 155–163 (2019).
- ²⁷S. Rajagopal, N. Sadhoo, and B. Zeqiri, "Reference characterisation of sound speed and attenuation of the IEC agar-based tissue-mimicking material up to a frequency of 60 MHz," *Ultrasound Med. Biol.* **41**(1), 317–333 (2015).
- ²⁸J. Pinkerton, "The absorption of ultrasonic waves in liquids and its relation to molecular constitution," *Proc. Phys. Soc. Sect. B* **62**(2), 129–141 (1949).
- ²⁹B. E. Treeby and B. T. Cox, "k-wave: MATLAB toolbox for the simulation and reconstruction of photoacoustic wave fields," *J. Biomed. Opt.* **15**(2), 021314 (2010).
- ³⁰W. Sachse and Y.-H. Pao, "On the determination of phase and group velocities of dispersive waves in solids," *J. Appl. Phys.* **49**(8), 4320–4327 (1978).
- ³¹W. Marczak, "Water as a standard in the measurements of speed of sound in liquids," *J. Acoust. Soc. Am.* **102**(5), 2776–2779 (1997).
- ³²J. F. Kelly, R. J. McGough, and M. M. Meerschaert, "Analytical time-domain green's functions for power-law media," *J. Acoust. Soc. Am.* **124**(5), 2861–2872 (2008).
- ³³B. E. Treeby and B. T. Cox, "Modeling power law absorption and dispersion for acoustic propagation using the fractional laplacian," *J. Acoust. Soc. Am.* **127**(5), 2741–2748 (2010).
- ³⁴K. R. Waters, J. Mobley, and J. G. Miller, "Causality-imposed (kramers-kronig) relationships between attenuation and dispersion," *IEEE Trans. Ultrason. Ferroelectr. Freq. Control* **52**(5), 822–823 (2005).
- ³⁵B. E. Treeby, E. Z. Zhang, A. S. Thomas, and B. T. Cox, "Measurement of the ultrasound attenuation and dispersion in whole human blood and its components from 0–70 mhz," *Ultrasound Med. Biol.* **37**(2), 289–300 (2011).
- ³⁶P. M. Morse and K. U. Ingard, *Theoretical Acoustics*. (Princeton University Press, 1986).
- ³⁷C. Li, L. Huang, N. Duric, H. Zhang, and C. Rowe, "An improved automatic time-of-flight picker for medical ultrasound tomography," *Ultrasonics* **49**(1), 61–72 (2009).
- ³⁸United Kingdom Accreditation Service, *The Expression of Uncertainty and Confidence in Measurement*, 3 ed., (UKAS, 2012), Vol. M3003, pp. 1–81.
- ³⁹JCGM/WG 1 - Working Group 1 of the Joint Committee for Guides in Metrology, "JCGM 100:2008 Evaluation of measurement data - Guide to the expression of uncertainty in measurement (GUM 1995 with minor corrections)," JCGM - Joint Committee for Guides in Metrology (2008), pp. 1–134.
- ⁴⁰Stratasys, "Stratasys: Our materials," <https://www.stratasys.com/-/media/files/printer-spec-sheets/polyjet-3d-printers-systems-materials-spec-sheet.pdf>.
- ⁴¹Formlabs, "Formlabs: Strandard resins," <https://formlabs.com/uk/materials/standard/#clear>.
- ⁴²S. Jiménez-Gambín, N. Jiménez, and F. Camarena, "Transcranial focusing of ultrasonic vortices by acoustic holograms," *Phys. Rev. Appl.* **14**(5), 054070 (2020).